

Flux-flow resistivity in UPt_3 : Evidence for nonsingular vortex-core structure

N. Lütke-Entrup,¹ R. Blaauwgeers,² B. Plaçais,¹ A. Huxley,³ S. Kambe,³ M. Krusius,² P. Mathieu,¹ and Y. Simon¹

¹Laboratoire de Physique de la Matière Condensée de l'ENS, UMR 8551, 24 rue Lhomond, F-75231 Paris Cedex 5, France

²Low Temperature Laboratory, Helsinki University of Technology, Box 2200, FIN-02015 HUT, Finland

³Département de Recherche Fondamentale sur la Matière Condensée, CEA, F-38054 Grenoble Cedex 5, France

(Received 23 March 2001; published 22 June 2001)

We have investigated the core structure of B -phase vortex lines in two clean UPt_3 crystals, using flux-flow dissipation as the probe. The flux-flow resistivity is determined from the skin depth of the high-frequency oscillations of the vortex lines in the pinned state. With $\hat{H} \perp \hat{c}$, our data agree with the previously established scaling law of the moderately clean limit with anisotropic gap. When $\hat{H} \parallel \hat{c}$, the resistivity is three times larger. We interpret this increase as evidence for a vortex-core structure with two length scales, as predicted for UPt_3 with a two-component order parameter.

DOI: 10.1103/PhysRevB.64.020510

PACS number(s): 74.60.Ge, 74.25.Nf, 74.25.Fy, 74.70.Tx

I. INTRODUCTION

Recent studies of the heavy-fermion superconductor UPt_3 are providing increasing support for odd-parity pairing, where the orbital symmetry belongs to the two-dimensional E_{2u} representation of the hexagonal group.¹ Its low-temperature B phase breaks time-reversal symmetry, with a nodal structure of the gap as $\Delta_{\pm} \sim k_z(k_x \pm ik_y)^2$, whereas the high-temperature A phase violates in-plane rotational invariance with $\Delta \sim k_z(k_x^2 - k_y^2)$. This change in symmetry is consistent with a rotation of the hexagonal flux-line lattice with respect to the crystal axes, which was observed to take place at the AB transition in recent neutron scattering experiments.² The upper critical field H_{c2} shows a paramagnetic limitation, when the external field \mathbf{H} is along the \hat{c} axis, which is characteristic of a spin-triplet state. The twofold orbital degeneracy ($\mathbf{L}_{0\pm} = \pm \hat{c}$) opens the possibility for the existence of unconventional nonsingular structures in the two-component order parameter field (η_+, η_-), such as domain walls or new vortex cores.³⁻⁵ A multitude of different vortex structures and other topological defects have been discovered in ^3He superfluids,⁶ but to our knowledge, their observation in superconductors is uncharted.

The size of such nonsingular structures is determined by a larger length scale $\tilde{\xi} = \xi/\sqrt{\beta}$, which is related to the superconducting coherence length ξ via the coupling coefficient β in the term $\beta|\eta_+ \eta_-|^2$, which breaks time-reversal symmetry in the two-dimensional Ginzburg-Landau functional.^{5,7} When the coupling is small ($\beta < 1$), $\tilde{\xi} \gg \xi$ leads to modifications in the vortex-core structure. Numerical calculations predict three different structures as function of β (and the coefficients of the gradient terms):⁷ the classical axisymmetric singular core at large β and, for $\beta \leq 0.25$, two nonaxisymmetric nonsingular cores (which are different for $\hat{\mathbf{H}} = +\hat{\mathbf{L}}_0$ and $\hat{\mathbf{H}} = -\hat{\mathbf{L}}_0$). In contrast to the former, in the latter two cases the order parameter amplitude does not go to zero anywhere within the core, which has a large radius $b \sim \tilde{\xi} \geq 2\xi$. With $\mathbf{H} \perp \hat{c}$, the coupling between the orbital and vortex momenta vanishes. Thus basal-plane vortices are expected to be classical, albeit distorted owing to the hexagonal anisotropy ($\xi_a \approx 0.6 \xi_c = 9 \text{ nm}$).

In this work, the vortex core is investigated by measuring the flux-flow resistivity $\rho_f(H)$ in clean samples, with a mean-free path $l_m \sim 500 \text{ nm}$. At low vortex density, $n = \mu_0 H / \varphi_0 \ll \xi^{-2}$, flux-flow dissipation is governed by the dynamics of localized core excitations, which are quasiballistic ($l_m \gg \xi$) and sensitive to the confining energy ($\omega_0 \propto \xi^{-2}$). Our measurements are performed in the B phase ($T = 0.1-0.3 \text{ K}$), with $\mathbf{H} \perp \hat{c}$ and $\mathbf{H} \parallel \hat{c}$, using a high-frequency skin-depth technique. With $\mathbf{H} \perp \hat{c}$ the results agree with previous dc measurements of flux-flow resistance⁸ and its scaling law⁹ in the low-field and low-temperature limit. In the $\mathbf{H} \parallel \hat{c}$ orientation, which was not investigated before, the resistivity exceeds the scaling result by a large factor $\rho_{\parallel} / \rho_{\perp} \approx 3$. The difference cannot be explained by material, scattering, and/or pairing anisotropy; but different vortex-core structures in the two crystal directions, as predicted by the odd-parity pairing theory, can readily account for the result.

II. VORTEX CORE RESISTIVITY

As discussed by Kopnin and Lopatin in moderately clean superconductors ($\xi \ll l_m \leq \xi E_F / \Delta$) flux-flow dissipation is proportional to the minigap ω_0 and the normal-state collision time τ .⁹ Taking axisymmetric vortices of radius $b = \xi$ and allowing for anisotropy in $\Delta(\mathbf{k}_F)$ over a spherical Fermi surface, they predict that

$$r^*(T) = \frac{1}{2\pi n b^2} \frac{\rho_f(H)}{\rho_n(H)} \approx \alpha \frac{k_B T_c}{\Delta_{\max}(T)} \quad (1)$$

for $\omega_0 \tau \leq 1$. The dimensionless factor $\alpha = \Delta_{\max}^2 / \langle \Delta^2(\mathbf{k}) \rangle$ accounts for gap anisotropy, and $\langle \rangle$ denote a Fermi-surface average, weighted by the factor $\frac{3}{2} [1 - (\hat{\mathbf{k}} \cdot \hat{\mathbf{H}})^2]$. For an isotropic gap (s -wave superconductor), α is unity, but it is larger than unity and has angular dependence, if $\Delta(\mathbf{k})$ has nodal structure. The previous dc measurements⁸ have verified the temperature dependence in Eq. (1), when $\mathbf{H} \perp \hat{c}$, and yield $\alpha = 3.2$. These basal plane vortices are classical, with $b^2 = \xi_a \xi_c$ and $\mu_0 H_{c2} = \varphi_0 / 2\pi \xi_a \xi_c$, so that r^* reduces to the experimental quantity $r_0 = (\rho_f / \rho_n)(H_{c2} / H)$. We shall see below that the situation with $\mathbf{H} \parallel \hat{c}$ is different.

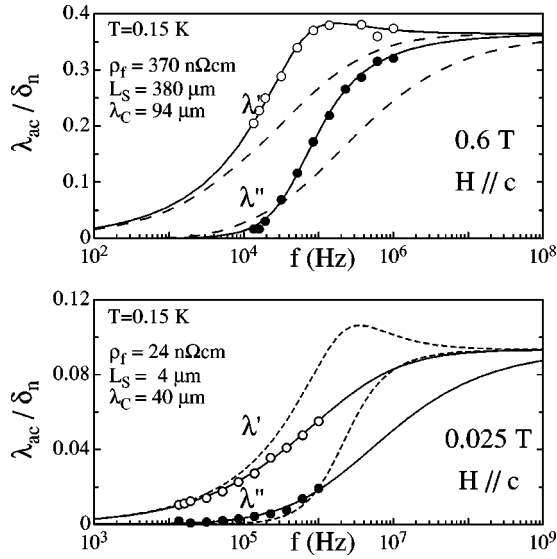


FIG. 1. Spectra of the apparent penetration depth $\lambda_{ac}(f) = \lambda' + i\lambda''$, showing as a function of frequency the crossover from pinning-dominated to free-flow response. The latter corresponds to the high frequency plateau, with $\lambda'' \approx \lambda' = \delta_f/2$. The solid curves are fits to Eq. (2) with L_S , λ_C , and ρ_f as adjustable parameters. To illustrate their relative influence on the fitting, the dashed curves represent pure bulk-pinning ($1/L_S = 0$) and the dash-dotted curves pure surface-pinning ($1/\lambda_C = 0$).

III. MEASUREMENT OF ac PENETRATION DEPTH

In the B phase the use of large dc currents, to unpin vortex lines and to bias the system into the free-flow state, is prohibited due to excessive Joule heating. Here this difficulty is overcome by measuring the complex penetration depth $\lambda_{ac}(f) = \lambda' + i\lambda''$ in the high-frequency range ($f = 0.01$ – 1 MHz) above the pinning frequency f_p , where a low dissipation level can be maintained (≤ 0.1 nW/mm²). In the overdamped regime $f \gg f_p$, which is achieved at intermediate and high fields, the rf-field penetration is restricted to within the free-flow skin depth and $\lambda' = \lambda'' = \delta_f/2 = \sqrt{\rho_f/(4\pi\mu_0 f)}$. Note that these frequencies are sufficiently low so that the anomalous-skin and relaxation-time effects can be ignored. At low fields, pinning is so strong that $f \sim f_p$. Even in this regime we can still extract reliable values for ρ_f by fitting [Eq. (2) below] to the measured resistive and reactive components of $\lambda_{ac}(f)$ (Fig. 1). This fitting procedure yields better accuracy and gives results for ρ_f over the full range of applied fields. Experimental details, as well as our methods of data taking and analysis, can be found in Ref. 10.

Measurements have been performed on two large single crystals (labeled $B22$ and $B3b$). They were prepared in Grenoble and were spark cut from the same ingot. Their quality is very similar to the sample of Ref. 8 and comparable to the best samples.^{11,12} After cutting, the crystals were annealed, but no surface polish was applied. Their final dimensions are $L(x) \times W(y) \times d(z) = 5.5(\hat{\mathbf{a}}^*) \times 2.9(\hat{\mathbf{a}}) \times 1.16(\hat{\mathbf{c}})$ mm³ ($B3b$), and $5.5(\hat{\mathbf{c}}) \times 3.04(\hat{\mathbf{a}}^*) \times 0.63(\hat{\mathbf{a}})$ mm³ ($B22$). They have low residual resistivity, $\rho_n = 0.52 + 1.44T^2 + 0.02(\mu_0 H)^2$ $\mu\Omega$ cm ($\mu_0 H$ in Tesla) for currents

$J \perp \hat{\mathbf{c}}$, and $\rho_n = 0.17 + 0.53T^2$ $\mu\Omega$ cm for $J \parallel \hat{\mathbf{c}}$ (and $H = 0$).

The dc field ($\mu_0 H \leq 3$ T) and the vortex lines are along the $\hat{\mathbf{z}}$ direction. The excitation field, $h e^{-i2\pi f t}$, is applied along the $\hat{\mathbf{x}}$ direction, so that the vortices oscillate in the xz plane close to the z -oriented surfaces, and electric fields \mathbf{E} are induced along the $\hat{\mathbf{y}}$ direction, so that penetrating currents are always perpendicular to the c axis. Owing to the Lorentz-force anisotropy, closing currents at the sample edges are superficial (within the London depth λ_L) and lead to negligible contributions in flux penetration. The measured signal is the flux Φ_{ac} through a 15-turn pick-up coil wound directly around the sample in the $\hat{\mathbf{x}}$ direction. The apparent complex penetration depth is defined as $\lambda_{ac} = [\Phi_{ac}(H) - \Phi_{ac}(0)] / (2\mu_0 h W)$.

The sample with its pick-up coil and the slightly larger excitation solenoid are placed inside the mixing chamber of a ³He-⁴He dilution refrigerator. The measurements are performed in the temperature range $T = 0.1$ – 0.3 K, by recording the spectrum $\lambda_{ac}(H)$ at fixed frequency f and by moving from one frequency value to the next, while the temperature is kept constant with a feedback loop. The temperature is monitored with a calibrated Ge resistance thermometer inside the mixing chamber. Its field dependence is adjusted by comparing the measured H_{c2} values with those in Ref. 13. The amplitude and phase of the signal voltage are calibrated against the difference between the responses in the normal-state ($\delta_n = 40$ – 400 μ m) and the Meissner state ($\lambda_L \sim 0.6$ μ m). This normalization procedure yields a phase accuracy better than 1° and a resolution $\delta\lambda_{ac} \leq 1$ μ m.¹⁰

Typical spectra of $\lambda_{ac}(f)$ are shown in Fig. 1. The complete data set consists of more than 200 different spectra. The real and imaginary parts of λ_{ac} can be accurately fit with the following formula:^{10,14}

$$\frac{1}{\lambda_{ac}} = \frac{1}{L_S} + \sqrt{\frac{1}{\lambda_C^2} - \frac{2i}{\delta_f^2}} \quad (2)$$

$L_S(H, T)$ and $\lambda_C(H, T)$ are two frequency-independent lengths, that describe surface and bulk pinning, respectively. The high-frequency limit, $\lambda_{ac}(f \rightarrow \infty) = (1 + i)\delta_f/2$, corresponds to the ideal flux-flow response, while the low-frequency limit, the quasistatic response $\lambda_{ac}(f \rightarrow 0) = \lambda'(0) = (\lambda_C^{-1} + L_S^{-1})^{-1}$, is purely inductive and cannot discriminate between surface and bulk pinning. The relative weight of surface and bulk pinning becomes apparent in the crossover regime.

IV. VORTEX PINNING

As explained in Ref. 10, the excitation field penetrates as the sum of two modes. The first one, localized near the surface, is associated with strong screening currents, whose amplitudes are governed by surface roughness. If the bulk sample is free of defects, the screened field penetrates further over the free-flow depth δ_f . This situation ($\lambda_C \rightarrow \infty$) has been systematically the case in the conventional superconductors, which so far have been measured.¹⁰ In contrast, if there are bulk defects, such as those usually introduced in

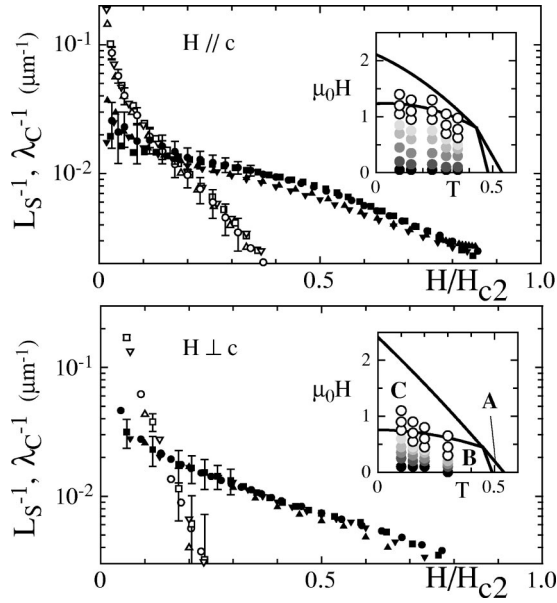


FIG. 2. Field dependence of the bulk and surface pinning strengths, $1/\lambda_C$ (solid symbols) and $1/L_S$ (open symbols) in two crystal orientations. The different symbols denote measurements at different temperatures below 0.33 K. The data are derived from fits to the measured $\lambda_{ac}(f)$ spectra, as shown in Fig. 1. Bulk pinning $1/\lambda_C$ vanishes at H_{c2} , while the surface contribution $1/L_S$ decreases more rapidly and vanishes just below the $B \rightarrow C$ transition. The surface-pinning fraction is shown in gray-scale units in the inset, together with the UPt_3 phase diagram as a function of field and temperature.

classical theories of pinning,¹⁵ the bulk mode is strongly attenuated, but penetrates at low frequencies over a Campbell length λ_C ($\ll \delta_f$ at low frequencies). Note that nonlocal vortex-creep corrections, considered in some theories, can be neglected here due to the high pinning frequencies of the UPt_3 samples.

In both crystal orientations vortex pinning is strong and is dominated by the surface process at low fields (Fig. 2). This is not surprising, since after spark cutting the surfaces are visibly rough. With increasing field, surface pinning falls down and finally vanishes at a field value close, but below the $B \rightarrow C$ transition. This result is consistent with recent observations in point contact spectroscopy,^{16–18} which suggest a suppression of the order parameter at the surface at higher fields. Our crystals also display a large bulk pinning strength $1/\lambda_C$, which decreases only slowly as a function of $(H_{c2} - H)$ and is the dominant source of pinning in the C phase. No clear anomaly can be distinguished at the $B \rightarrow C$ transition.¹⁴ Nor do we observe hysteresis as a function of the field-sweep direction. Low-field vortex-creep measurements¹⁹ have suggested that new pinning mechanisms could be present, such as intrinsic pinning by domain walls in the bulk.³ If this is the source for the unusually large bulk pinning, then the domain walls have to persist in the C phase. On the other hand, we cannot exclude that more microscopic defects, such as stacking faults in the crystal lattice, which are known to control the residual resistivity in clean UPt_3 samples,¹¹ might also play a role in bulk pinning.

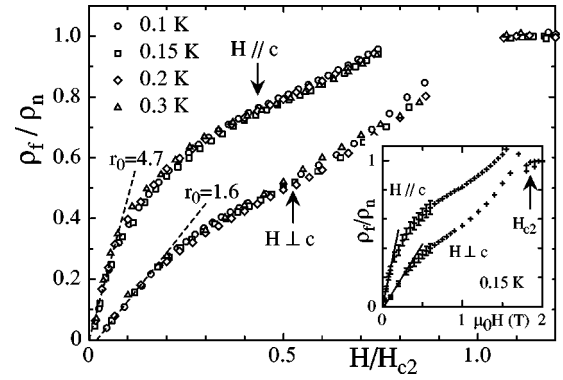


FIG. 3. Flux-flow resistivity $\rho_f(H)$, as deduced by fitting the measured $\lambda_{ac}(f)$ (Fig. 1) to Eq. (2). The data show that $\rho_f(H)$ becomes temperature independent below 0.3 K as a function of H/H_{c2} . The results differ when measured with $\mathbf{H} \parallel \hat{c}$ (sample B3b) or $\mathbf{H} \perp \hat{c}$ (sample B22). The limiting low-field low-temperature slope is denoted with r_0 , assuming the linear relation $\rho_f/\rho_n = r_0(H/H_{c2})$. The dashed lines define the fitted values $r_{0\perp} = 1.6 \pm 0.15$ and $r_{0\parallel} = 4.7 \pm 0.3$. The inset shows unscaled data at 0.15 K and illustrates that H_{c2} coincides in the two directions. The overshoot in ρ_f just below H_{c2} is an artifact due to the onset of flux penetration at the edges of the sample. In the main frame as well as in Fig. 2 such data points have been omitted.

Additional work, in particular, variations in surface treatment, should provide better insight in the pinning processes.

V. FLUX-FLOW RESISTIVITY

The flux-flow resistivity is deduced from the high-frequency extrapolation of the ac penetration depth to the free-flow limit $\lambda' = \lambda'' = (\rho_f/4\pi\mu_0f)^{0.5}$, which correspond to the plateaus in Fig. 1. The normalized resistivity, ρ_f/ρ_n , is shown in Fig. 3. A characteristic of the moderately clean superconductor appears to be that $\rho_f(H)$ tends to exceed the “normal-core limit,” $\rho_f = \rho_n H/H_{c2}$, as was already noted in Ref. 8. In the direction $\mathbf{H} \perp \hat{c}$, where comparison is possible, $\rho_f(H)$ agrees quantitatively with the earlier dc measurements of Ref. 8. At low field the scaling factor $r_0(T)$ tends to the value $r_{0\perp} = 1.6 \pm 0.15$ in the low-temperature limit. In fact, as seen in Fig. 3, below $0.3 \text{ K} \approx 0.6T_c$, r_0 is already temperature independent. This is in agreement with the results in Ref. 8, when these are extrapolated to low temperatures, and testifies for good general consistency between two different measuring methods and samples. If we take $\Delta_{\max}(0) = 1.9k_B T_c$ from Ref. 16 and put $r^* = r_0$ in Eq. (1), then we get $\alpha_{\perp} = 1.6 \times 1.9 \approx 3.0$, which agrees within the combined experimental precisions with the value 3.2 obtained in Ref. 8. This large value of α arises from gap anisotropy.

An analysis of the measurements in terms of Eq. (1) applies for conventional superconductors with $r_0 = r^*$, or equivalently, $b_{\perp}^2 = \xi_a \xi_c = \varphi_0 / (2\pi\mu_0 H_{c2\perp})$. Here, however, $H_{c2\parallel}$ is not a good scaling parameter because of the Pauli paramagnetic limitation at low temperatures in this direction. To compare the results in the two orientations, we assume that the effective core radii are $b_{\perp}^2 = \xi_a \xi_c$ and $b_{\parallel}^2 = \xi_a^2$. From the high-temperature anisotropy we get $\xi_a = 0.6 \xi_c$. In the

perpendicular orientation we set r_{\perp}^* equal to its measured value $r_{0\perp} = 1.6$, while in the axial direction we then have $r_{\parallel}^* = r_{0\parallel}(\xi_c/\xi_a) = 7.8$. Equation (1) shows that these correspond to $\alpha_{\perp} = 3.0$ and $\alpha_{\parallel} = 7.8 \times 1.9 = 14.8$, which represents a large anisotropy of $\alpha_{\parallel}/\alpha_{\perp} \approx 5$.

An anisotropy in α as large as this cannot be explained by the UPt₃ structure, by taking into account the possible anisotropies from the D_{6h} point group symmetry in the expression of α in Eq. (1). For E_{1g} with a nodal structure $\Delta \sim k_z(k_x \pm ik_y)^2$ we find $\alpha_{\parallel} = 1.25 \alpha_{\perp} = 4.4$. There is no anisotropy at all associated with the E_{2u} symmetry and $\alpha_{\parallel} = \alpha_{\perp} = 3.9$. Thus the small jump of about 10% in ρ_f/ρ_n , which was observed in Ref. 8 at the $A \rightarrow B$ transition for in-plane vortices ($\mathbf{H} \perp \hat{\mathbf{c}}$), might be ascribed to the combined anisotropy in crystal structure and symmetry breaking, but not our large value of $r_{0\parallel}/r_{0\perp}$.

Quasiparticle scattering may additionally contribute to the anisotropy in $\rho_f(\mathbf{H})$. An estimate can be worked out by comparing the anisotropy in $\rho_n(\mathbf{J})$ to that in the slope of the critical field $H_{c2}(T)$ at T_c : $[dH_{c2}/dT]_{\parallel} \approx -7.2$ T/K and $[dH_{c2}/dT]_{\perp} \approx -4.6$ T/K.¹² These values yield $\gamma = \xi_a/\xi_c \approx 0.64$, which corresponds to an effective mass ratio of $m_c^*/m_a^* = \gamma^2 \approx 0.41$. The anisotropy in $\rho_n(\mathbf{J})$ amounts to a ratio $\rho_{n\parallel}/\rho_{n\perp} \approx 0.33-0.37$. This value includes the anisotropies in effective masses and in quasiparticle relaxation times. Comparing the two estimates we conclude that the anisotropy in quasiparticle scattering is of order $\sim 10\%$, in agreement with the estimates in Ref. 11.

Finally, one more source of anisotropy is a different vortex core structure in the two orientations. The large ρ_f/ρ_n in

Fig. 3, measured with $\mathbf{H} \parallel \hat{\mathbf{c}}$, can then be explained by assuming $r_{\parallel}^* = r_{\perp}^*$ and $b_{\parallel}^2 = 3 b_{\perp}^2 = 3 \xi_a \xi_c$, rather than $b_{\parallel}^2 = \xi_a^2$, as was done above. If we ascribe in this way the entire measured anisotropy to an increase in the effective core radius in the axial orientation and take $b_{\parallel} = \tilde{\xi}$, we estimate the Ginzburg-Landau coefficient to be $\beta = \xi_a^2/\tilde{\xi}^2 \approx 0.2$. This value falls within the regime of the nonaxisymmetric core structures,⁷ while with $\beta \geq 0.25$ the axisymmetric core would be favored. Such a result for β is also in agreement with the determination $\beta \sim 0.2-0.5$, which was extracted from the specific-heat jump at T_c .²⁰ For better quantitative comparison, Eq. (1) for the flux-flow resistivity needs to be reconsidered to account for the actual core structures.

In summary, our measurements provide indication for an unconventional vortex-core structure in UPt₃. The effective core radius in the axial orientation appears to be two times larger than for vortex lines oriented along the basal plane, i.e., their radius acquires the value $\tilde{\xi} \approx \sqrt{3 \xi_a \xi_c} \approx 2 \xi_a$. This is possible if the ‘‘hard vortex core’’ has reduced rotational symmetry, as is known to be the case for the dumbbell-like double-core vortex in ³He-B at low temperatures.⁶

ACKNOWLEDGMENTS

We acknowledge instructive discussions with N. Kopnin and J. Flouquet. N.L.-E. and B.P. thank the LTL for hospitality. This work was funded partly by the EU Improving Human Potential Program (Contract No. EC HPRI-CT-1999-50). The UMR 8551 is ‘‘Unité Mixte de Recherche’’ of the CNRS, associated with universities Paris 6 and Paris 7.

- ¹M.J. Graf, S.-K. Yip, and J.A. Sauls, *Physica B* **280**, 176 (2000); *Phys. Rev. B* **62**, 14393 (2000).
- ²A. Huxley, P. Rodière, D. MacPaul, N. van Dijk, R. Cubbit, and J. Flouquet, *Nature (London)* **406**, 160 (2000).
- ³M. Sigrist and K. Ueda, *Rev. Mod. Phys.* **63**, 239 (1991).
- ⁴J.A. Sauls, *Adv. Phys.* **43**, 113 (1994).
- ⁵I.A. Luk'yanchuk and M.E. Zhitomirsky, *Supercond. Rev.* **1**, 207 (1995).
- ⁶V.B. Eltsov and M. Krusius, in *Topological Defects in ³He Superfluids and the Non-equilibrium Dynamics of Symmetry-Breaking Phase Transitions*, edited by Yu. Bunkov and H. Godfrin (Kluwer Academic, Dordrecht, 2000), p. 325.
- ⁷T.A. Tokuyasu, D.W. Hess, and J.A. Sauls, *Phys. Rev. B* **41**, 8891 (1990).
- ⁸S. Kambe, A.D. Huxley, P. Rodière, and J. Flouquet, *Phys. Rev. Lett.* **83**, 1842 (1999).
- ⁹N.B. Kopnin and A.V. Lopatin, *Phys. Rev. B* **51**, 15291 (1995); *J. Low Temp. Phys.* **110**, 885 (1998).
- ¹⁰N. Lütke-Entrup, B. Plaçais, P. Mathieu, and Y. Simon, *Phys. Rev. Lett.* **79**, 2538 (1997); *Physica B* **255**, 75 (1998); *Ann. Phys. (Paris)* **25**, 1 (2000).
- ¹¹J.B. Kycia, J.I. Hong, M.J. Graf, J.A. Sauls, D.N. Seidman, and W.P. Halperin, *Phys. Rev. B* **58**, R603 (1998).
- ¹²H. Suderow, J.P. Brison, A. Huxley, and J. Flouquet, *Phys. Rev. Lett.* **80**, 165 (1998).
- ¹³S. Adenwalla, S.W. Lin, Q.Z. Ran, Z. Zhao, J.B. Ketterson, J.A. Sauls, L. Taillefer, D.G. Hinks, M. Levy, and B.K. Sarma, *Phys. Rev. Lett.* **65**, 2298 (1990).
- ¹⁴N. Lütke-Entrup, R. Blaauwgeers, B. Plaçais, P. Mathieu, Y. Simon, M. Krusius, S. Kambe, and A. Huxley, *Physica B* **284-288**, 527 (2000).
- ¹⁵J.I. Gittleman and B. Rosenblum, *Phys. Rev. Lett.* **16**, 734 (1966); A.M. Campbell, *J. Phys. C* **2**, 1492 (1969).
- ¹⁶Y. De Wilde, J. Heil, A.C.M. Jansen, P. Wyder, R. Deltour, W. Assmus, A. Menovsky, W. Sun, and L. Taillefer, *Phys. Rev. Lett.* **72**, 2278 (1994).
- ¹⁷G. Goll, C. Bruder, and H.v. Löhneysen, *Phys. Rev. B* **52**, 6801 (1995).
- ¹⁸C. Obermair, G. Goll, H.v. Löhneysen, I.K. Yanson, and L. Taillefer, *Phys. Rev. B* **57**, 7506 (1998).
- ¹⁹A. Amann, A.C. Motta, M.B. Mapple, and H.v. Löhneysen, *Europhys. Lett.* **33**, 303 (1996).
- ²⁰R.A. Fisher, S. Kim, B.F. Woodfield, N.E. Phillips, L. Taillefer, K. Hasselbach, J. Flouquet, A.L. Giorgi, and J.L. Smith, *Phys. Rev. Lett.* **62**, 1411 (1989).